09

Developed Ag nanostructures on c-Si as surface-enhanced Raman scattering substrates for detection of triphenylmethane dye

© K.V. Prigoda,[1] A.A. Ermina,[1] V.O. Bolshakov,[1] V.S. Levitskii,[2] N.A. Belskaya,[1] D.P. Markov,[1] Yu.A. Zharova[1]

[1] Ioffe Institute,
194021 St. Petersburg, Russia
[2] Research and Engineering Center of Thin-film Technologies in Power Engineering
194064 St. Petersburg, Russia
e-mail: piliouguina@mail.ioffe.ru

Received April 23, 2024
Revised April 23, 2024
Accepted April 23, 2024

Dendritic silver nanostructures on silicon as surface-enhanced Raman scattering substrates are considered in this work. The structures were obtained by chemical reduction of $AgNO_3$ on the silicon surface with different metal deposition time. Positions of „hot spots“ of the structures under study was determined qualitatively by means of simulation in COMSOL Multiphysics, and enhancement factors from the structures were calculated $\sim 10^7$. The surface-enhanced Raman spectroscopy has shown reliable detection of aqueous solution of brilliant green dye on the prepared substrates. Limit of detection of the dye was 10^{-12} M. Using the experimental data, we have determined the enhancement factors reaching 10^8 for the least developed structure and 10^7 for more developed structures.

Keywords: surface-enhanced Raman scattering, Ag nanodendrites, silicon, hot spots, brilliant green.

DOI: 10.61011/TP.2024.07.58811.128-24

Introduction

Waste water contamination with dyes is currently a serious problem because they can affect both the environment and human health [1,2]. There is a multitude of various dyes that are widely used in food, pharmaceutical, beauty, printing, dye and textile industries, and in aquaculture [1–5]. The study investigates a synthetic aniline triphenylmethane dye — brilliant green. This dye is used as local antiseptic, dermatological product, bird feed additive against mould, intestinal parasites and fungi, and for textile and paper dyeing [6,7]. In terms of its chemical structure, i.e. the nature of chromophoric groups, the triphenylmethane series is assigned to the polymethine dye subgroup [5,8], i.e. dyes containing more than one methine group. Such dyes were previously widely used as bactericides [9], e.g. against fungal and parasitic infections of fish due to their efficacy, availability and low cost [10]. When this series of dyes had been found to be toxic, their applications in various countries were limited considerably or prohibited [11]. These dyes even in low concentrations can be cancerogenic and mutagenic for living beings [7,12]. Some dye residues are still found in seafood and waste water [4,10], therefore, it is important to identify molecules of such dyes at low concentrations in various biological analytes (for example, for water analysis).

In recent decades, most of researchers have been focused on the development of various water treatment methods used to remove dye waste [5,6,12–14]. The authors of [15] describe in detail various treatment methods that are currently proposed: from activated carbon to photocatalytic oxidation. However, identification of dyes in various biological samples is the top-priority task: both in water samples and in animal tissues. There are numerous triphenylmethane dye detection methods: electrochemical [16], electroluminescent [17], immunoenzymometric [18], liquid chromatography [11,19], mass-spectrometry [10], and Raman scattering spectroscopy [20–22], etc.

Surface-enhanced Raman spectroscopy (SERS) is one of the most sensitive non-destructive test methods to detect various analytes with high response rate [23–26]. This allows ultra-low amount of substances up to individual molecules to be detected and studied on various substrates [27]. SERS method provides enhancement of the Raman scattering signal from the test sample. This may be achieved, first, by localized plasmon resonance excitation on a custom-made substrate by the external electromagnetic wave and, consequently, by occurrence of plasmon effects. Second, the Raman scattering signal on various, usually metallic, nanostructures may be enhanced due to the presence of „hot spots“ [28]. Highly morphologically developed structures more likely might have multiple „hot spots“ and, consequently, high Raman scattering enhancement factor (EF) [29].

In recent years, increasingly greater attention has been drawn to the SERS spectroscopy, therefore, the use of the SERS substrates for a wide variety of applications has increased dramatically. For example, they are used in biological and medical testing to detect and study viruses, cells, proteins, tissues and DNA [30–33], and in forensics

for identification of banned and hazardous substances or for authentication of products [34]. They may be also used in environmental studies to detect contaminants and toxic dyes [21,35–40] and in food industry (pesticide test, etc.) [38,41–43]. There are numerous SERS structures with different morphology, they may be: metallic nanoparticles deposited onto a substrate [44,45]; hybrid structures into which nanoparticles or nanofilms of one or more metals are embedded using various methods [40,46,47]; structures in the form of metal „nanoflowers“ [48–50]; dendritic metallic structures [31,51,52]. Silver and gold are the best metals for fabrication of SERS structures [53–55].

This study describes silver dendritic structures on silicon used as SERS substrates. Thanks to the well-developed morphology of the dendritic structure, intensity of a local electromagnetic field grows dramatically due to the presence of „hot spots“ that occur: 1) on sharp large-curvature tips on dendritic structure trunks and branches that act as a „lightning rod“; 2) on nanometer-scale gaps between neighboring branches and leaves of the dendritic structure. Therefore, silver dendrites are nanostructures with multiple „hot spots“ that in turn play a major role in the Raman scattering enhancement. Silver was chosen because it is chemically stable, easily synthesized and is much cheaper than other noble metals used for fabrication of SERS substrates. Various detectable substances (analytes) are also absorbed on the silver surface more likely than on other noble metals [56], which is an advantage of silver. We propose a simple and reproducible SERS structure fabrication method that does not require any expensive equipment. Chemical reduction of silver nitrate on the silicon surface is used to create dendritic metallic nanostructures with uniform distribution over the area and structure morphology control due to varying the deposition time and solution concentration. Silicon was used as a substrate primarily because it is neutral to analyte molecules in most cases. In the method proposed herein, silicon is a reducing agent, more precisely, silver and silicon form a redox pair in this process. Thus, silicon participates in the oxidation-reduction reaction on its own, therefore, a part of its surface is etched to ensure good adhesion between silver and substrate [54]. Using the SERS spectroscopy, we studied the response from the fabricated structures with brilliant green aqueous solution applied to their surfaces at ultra-low concentration, and determined EF or each sample. Positions „hot spots“ positions and numerical EF were determined qualitatively using numerical simulation.

1. Experimental methodology

1.1. Nanostructure fabrication

p-type single crystal silicon (*c*-Si) with a resistivity of $10\,\Omega\cdot$cm, crystal-lattice orientation (111) was used as a substrate for fabrication of silver dendritic structures. After standard RCA (Radio Corporation of America) cleaning, the Si wafers were placed in 0.02 M $AgNO_3 + 5$ M HF solution at the volume ratio of 5:1. In this solution, silver is reduced on the Si wafer surface and dendritic nanostructures are formed. To create dendritic structures with different morphology, solution treatment time was set to — 40 s (sample S1), 60 s (sample S2) and 90 s (sample S3) at room temperature. Figure 1 shows schematically all experiment phases: Si wafer cleaning, dendritic nanostructure formation, analyte application (synthetic aniline triphenylmethane dye — brilliant green (BG) was used herein), analysis of analyte on the silver dendritic structure surface by the Raman scattering method and data analysis.

1.2. Characterization of nanostructures

Morphological analysis of the hybrid structures was performed using the JSM-7001F (JEOL, Japan) scanning-electron microscope (SEM) in secondary electron mode at an accelerating voltage of 5 keV. Statistical analysis of nanostructures was performed using SEM images and ImageJ open source image processing software.

X-ray diffraction analysis was performed using the DRON-8N (IC „Berevestnik“, Russia) X-ray diffractometer in the Bragg-Brentano geometry with the angle 2θ range from 30 to 67 deg. The diffractometer is equipped with an X-ray tube with Cu anode, BDS-25-10 (IC „Burevestnik“, Russia) scintillation point detector and one parabolic curved Gebel's mirror placed on the beam path such that the X-ray source focusing line is straight. Scanning was performed in continuous mode at a rate of 1 deg/min.

The Raman scattering spectra were measured using the Labram HR800 spectrometer (HORIBA, France) equipped with 633 nm radiation generating laser with a power of $1.6\,\mu$W to prevent analyte damage. A 600 lines/mm grating was used for the measurements, and the Olympus $100\times$ (NA = 0.9) lens was used to focus the laser beam on the sample surface into a spot with a diameter of $\sim 1\,\mu$m. Raman scattering measurement repeatability was provided by scanning the spot area from analyte on the $30\times 40\,\mu$m SERS substrate at the interval of $5\,\mu$m.

2. Results

2.1. Morphologies of fabricated substrates

Figure 2 shows SEM images of the fabricated Ag dendritic nanostructures on *c*-Si substrate. These images were used to calculate the average Ag layer thickness on all substrates: for sample S1 — 259 nm, for sample S2 — 627 nm, for sample S3 — 1084 nm. The figure clearly shows how the Ag structure morphology develops from stand-alone main „trunks“ (sample S1) to „trunks with multiple symmetric branches and leaves“ (samples S2 and S3), which increases the specific area of the Ag structure dramatically. In our previous studies [57–59], we studied optical properties and morphology of structures obtained by Ag deposition on a Si substrate from 0.02 M $AgNO_3 + 5$ M HF (1:1) solution during 30 s. In such deposition mode,

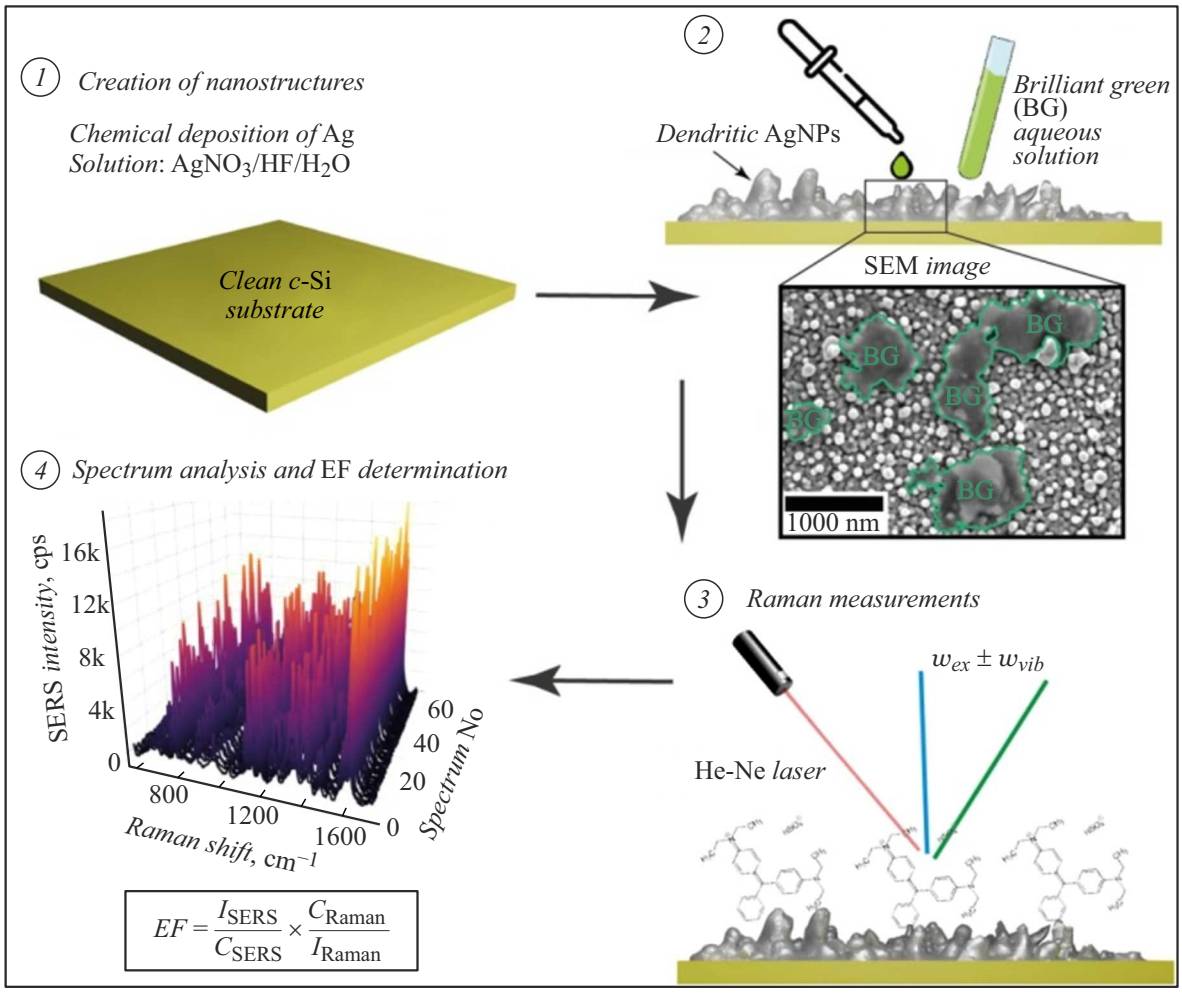

Figure 1. Scheme of the main experiment stages. *1* — preparing Si wafer and creating Ag dendritic nanostructures; *2* — applying the dye (BG); *3* — testing by the Raman scattering method; *4* — test data analysis.

formation of dendritic structures was not observed, and island Ag films with a mean thickness of 40–45 nm were produced.

Chemical deposition of Ag on the Si wafer from aqueous solution containing Ag^+ and HF is based on the electrochemical oxidation-reduction reaction when anodic and cathodic processes take place simultaneously on the Si surface [60]. Electrochemical reactions are represented by the following equations:
anodic

$$Si + 6HF = H_2SiF_6 + 4H^+ + 4e^-, \quad (1)$$

cathodic

$$Ag^+ + e^- = Ag. \quad (2)$$

In the reactions listed above, e^- denotes an electron. H_2SiF_6 is a soluble compound, therefore, reaction (1) is a reaction of Si removal by etching. Meanwhile, reaction (2) is a reaction of ionic Ag reduction to atomic Ag on *c*-Si surface.

It is known that covering the Si wafer surface by dendritic nanostructures and development of these structures depends on $AgNO_3$ concentration in the solution [60,61] or on the deposition time [62,63], the dendritic Ag structure morphology may vary depending on the deposition method: chemical deposition or electrochemical deposition under voltage [61]. For several years, authors of [54,61,64] have been investigating and comparing chemical and electrochemical methods of Ag deposition on Si surface, describing various conditions and silver-containing electrolytes, demonstrating different dendritic structure morphologies, and showing that dendritic nanostructures produced by electrochemical deposition are more developed than those produced by chemical deposition.

For this, the diffusion-limited aggregation model and anisotropic crystal growth are used to describe the dendritic Ag structure growth and development mechanism [62,65–67]. The dendritic structure formation process is described as follows: Ag particles undergoing Brownian motion in a solution find low-energy areas on the substrate, are deposited on it and start sticking together forming an initial, i.e. nucleation layer of Ag nanoparticles. Such layer can be observed within low deposition times or very low Ag

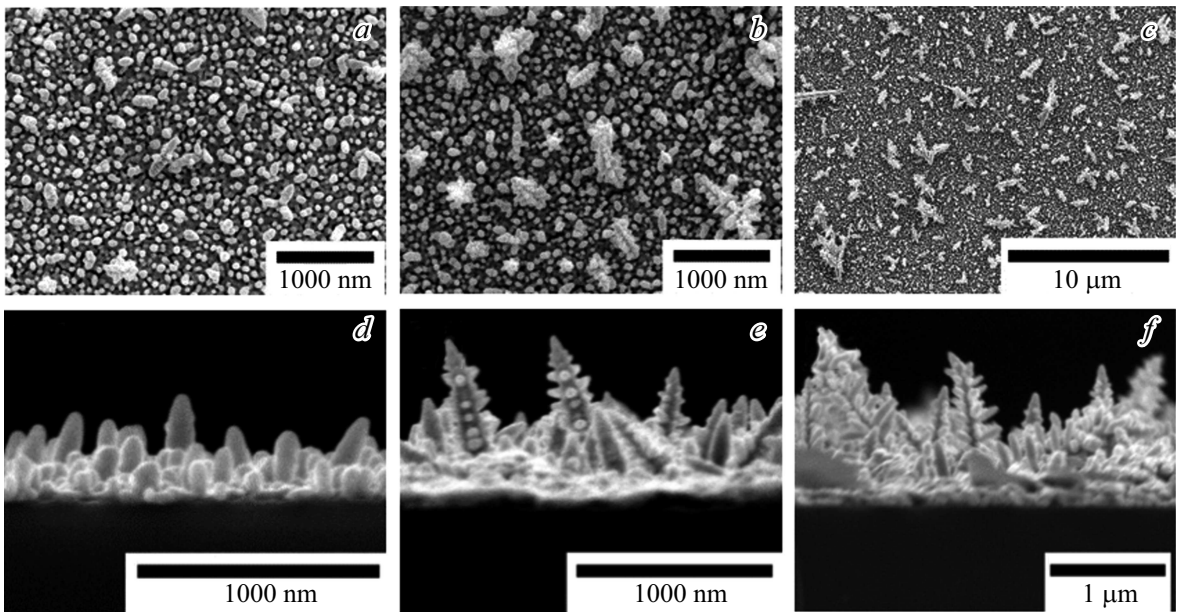

Figure 2. SEM images of Ag dendritic structures. Top view: S1 (*a*), S2 (*b*), S3 (*c*). Cross-section view: average height of structures S1 — 259 (*d*), S2 — 627 (*e*), S3 — 1084 nm (*f*).

concentrations in solution, when the silver nanoparticles completely or almost completely form an island layer on the Si wafer surface. As the time of treatment in the electrolyte containing a sufficient amount of Ag (as in case of diffusion from an inorganic source) grows or when a solution with high concentrations (excess concentration) is used, free nanoparticles will continuously diffuse to the produced nucleation layer forming more coarse particles, and then, when colliding with each other followed by aggregation, will form dendrites.

It is known that the morphology of the resulting nanoparticles is defined by different growth rate of crystal faces. Since silver is a metal with face-centered cubic lattice, the growth mechanism is more efficient in ⟨111⟩ orientations than in other orientations. Thus, at the initial stage, Ag nanoparticles will grow along ⟨111⟩ orientation forming a rod-like Ag trunk (sample S1). Then, growth of a structure with attachment of new particles to the trunk continues, these attached Ag nanoparticles also start growing in [111] orientation with formation of further secondary (sample S2) and tertiary branches (sample S3). As the reaction is executed, all trunks, branches and leaves become larger, thicker and denser, and form ordered, well-oriented Ag dendritic nanostructures. For Ag dendritic nanostructure formation, both diffusion control and oriented growth process play an important role.

2.2. X-ray diffraction (XRD) analysis

XRD patterns of the formed Ag dendritic structures are shown in Figure 3. The experimental XRD pattern shows a set of Bragg reflection peaks at 2θ of 37.8, 43.9 and 64.2 deg corresponding to (*hkl*) — (111), (200) and (220) planes.

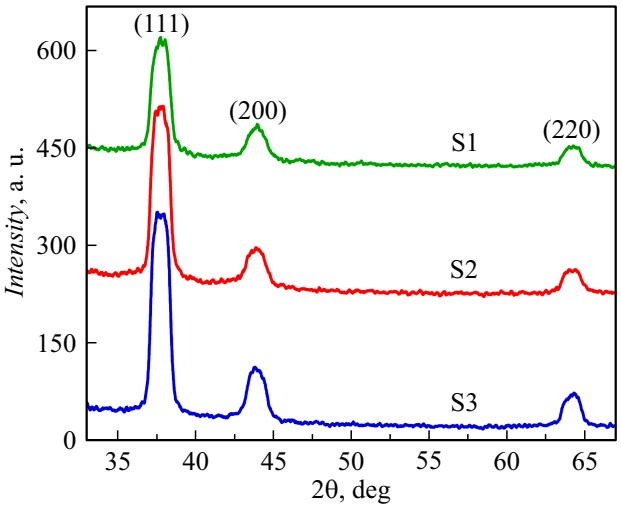

Figure 3. XRD patterns of the dendritic Ag nanostructures (samples S1, S2 and S3).

The XRD examination has confirmed that silver dendritic structures are Ag with face-centered cubic crystal structure (JCPDS, file No. 9008459) [68]. Thus, Ag nanoparticles are in metallic phase without impurities. As the amount of Ag increases, XRD intensity on samples grows indicating the growth of the degree of crystallinity.

2.3. Raman spectroscopy

Before SERS examination of Ag dendrites with applied BG aqueous solution, Raman scattering measurements of the initial *c*-Si wafer and Ag dendritic nanostructures on

c-Si without dye were performed. All spectra show a line near 520 cm $^{-1}$ corresponding to scattering on optical phonons of the first-order *c*-Si crystal lattice and a less intense Raman scattering band of the second-order *c*-Si (940–980 cm^{-1}) [40,69]. Also, the spectrum from Ag dendritic nanostructures clearly shows an intensive band at $\sim 240\,cm^{-1}$ caused by Ag-N bond stretching [70].

A drop (10 μl) of BG aqueous solution with different concentrations was applied to each substrate, then it was dried in air within 2 h. Figure 4 shows averaged values of 63 SERS spectra for the test samples with applied BG aqueous solution at concentrations 10^{-11}, 10^{-10}, 10^{-8} and 10^{-7} M on S1, S2 and S3 substrates. The SERS spectra clearly show all characteristic „fingerprints“ of BG [71]. The principal bands on 1616, 1593, 1491 and 1288 cm^{-1}

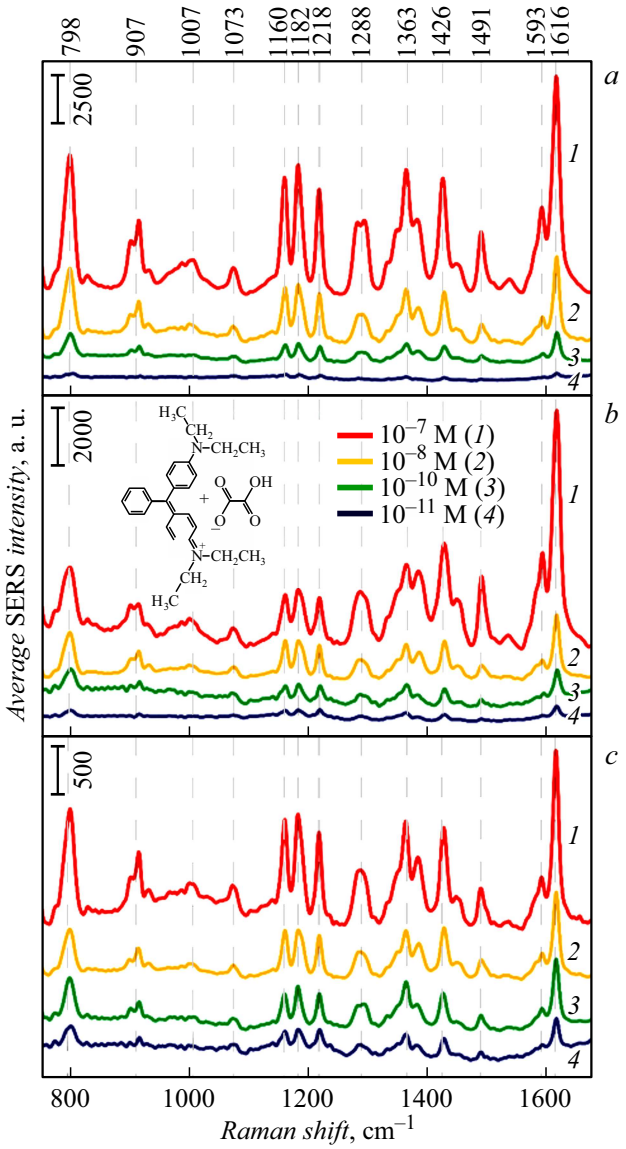

Figure 4. Averaged SERS spectra for samples S1 (*a*), S2 (*b*), S3 (*c*) with BG aqueous solution with concentrations: *1* — 10^{-7}, *2* — 10^{-8}, *3* — 10^{-10}, *4* — 10^{-11} M. Intensity scale is shown for each sample.

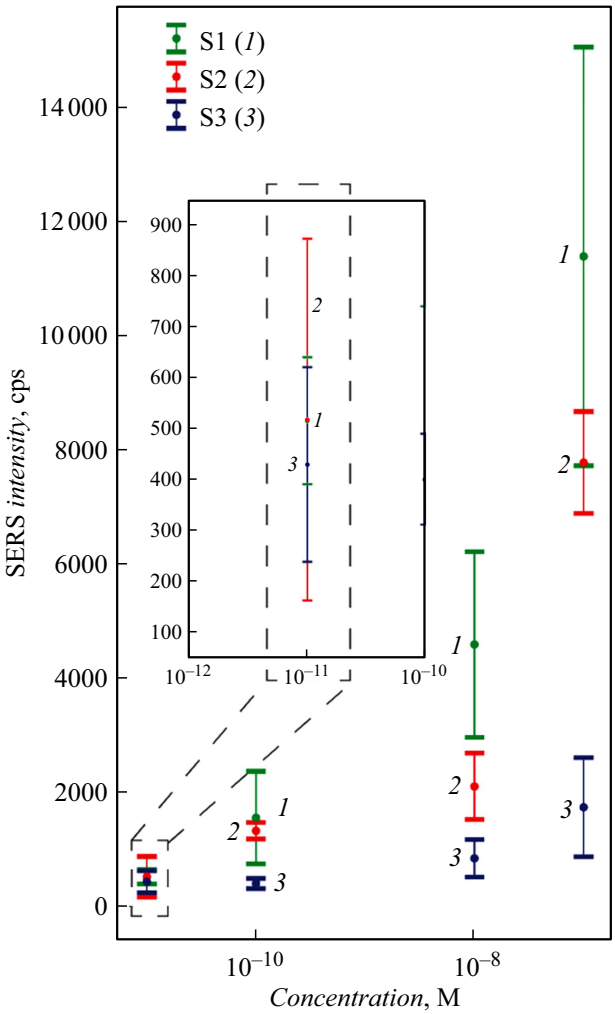

Figure 5. SERS intensity depending on BG aqueous solution concentration with standard deviation. Curve *1* — sample S1, *2* — S2, *3* — S3.

correspond to ν(C–C) ring stretching. Peaks at 1426 and 1363 cm^{-1} correspond to ν(N–ph) stretching + ν(N–ph) ring oscillation and stretching, respectively. And peaks at 1182, 1162, 1007 and 905 cm^{-1} correspond to in-plane bending of (C–H) ring. The highest intensity of the SERS signal is observed from sample S1 and then from S2. Substrate S3 demonstrates the lowest intensity, two reasons are possible: 1) dendritic structure becomes highly branched with time, and the Raman signal becomes weaker due to denser branches, gaps between dendrites decrease considerably, thus, reducing the number of „hot spots“ in the sample and affecting the Raman scattering characteristics; 2) high dendritic structure thickness ($\sim 1\,\mu$m) shields the signal from BG that has been absorbed into the depth to the dendritic bases. Although S1 is less morphologically developed compared with S2 and S3, its height turned out to be more effective for absorbing BG crystals. Concentration of 10^{-12} M was also applied to the structures, SERS intensity was ~ 10 cps on all structures.

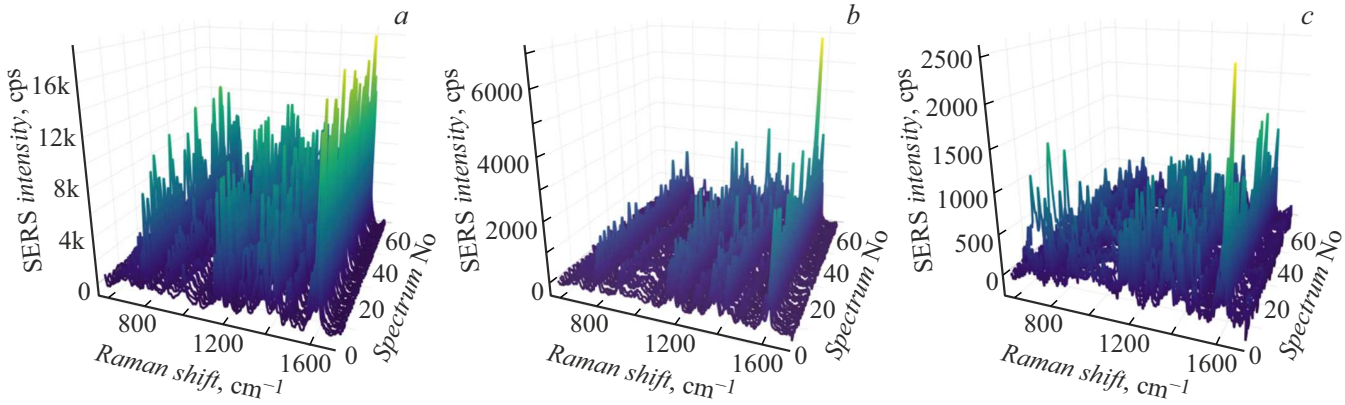

Figure 6. 3*D* SERS spectra from S1 (*a*), S2 (*b*), S3 (*c*) with BG aqueous solution (10^{-7} M) measured on an area of $30 \times 40\,\mu$m at $5\,\mu$m interval.

Thus, BG limit of detection from the structures studied herein is equal to 10^{-12} M.

Figure 5 shows the dependence of intensity of all SERS spectra measured on the test samples with the most intense peak 1616 cm^{-1} on BG aqueous solution concentration with standard deviation shown by error bars. For sample S1, standard deviation of the SERS signal is much higher compared with other samples.

For illustration, Figure 6 shows all spectra measured on area of $30 \times 40\,\mu$m at $5\,\mu$ interval from all test samples with a concentration of 10^{-7} M. There are individual peaks whose intensity is twice as high as the signal intensity across the measured area and distorts the general signal pattern from the analyte. This may be because laser falls on the analyte spot edge („coffee ring“). It is well known that self-induced drying of some liquid drops on particular hard surfaces forms a „coffee ring“ pattern [72].

The enhancement factor (EF) that can provide quantitative estimate of substrate efficiency in Raman signal increase from this molecule is a very important parameter that shall be considered when using SERS substrates. Analytical EF was calculated using the average values of the most pronounced peak at 1616 cm^{-1} using the following equation [73]:

$$\mathrm{EF} = \frac{I}{C}\frac{C_0}{I_0}, \tag{3}$$

where I and I_0 are intensities of signals from the analyte on the SERS substrate and pure c-Si wafer, respectively; C and C_0 are the analyte concentration applied to the SERS substrate and pure c-Si wafer, respectively.

Considering the analyte concentration 10^{-7} M, we have the mean SERS signal intensity 11375, 7767 and 1732 a.u. for S1, S2 and S3, respectively. Analyte with concentration 10^{-3} M was applied to c-Si , however, note that no response was seen due to luminescence, therefore the Raman signal intensity is assumed as 1 a.u. Thus, EF for S1 is equal to $1.14 \cdot 10^8$, for S2 is equal to $7.8 \cdot 10^7$, and for S3 is equal to $1.73 \cdot 10^7$. Calculations of numerical EF are shown below.

2.4. Numerical calculation

EF was calculated numerically in COMSOL Multiphysics commercial software using the finite element method. A 3D model with periodic boundary conditions along the x and y axes was developed (Figure 7). The incident field is a plane wave with normal incidence along the z axis. Perfectly matched layers (PML) were used on the top and bottom of the model in order to ignore the wave rereflection from the boundaries. The model shape was nominally set by the SEM image (Figure 2, *e*). The dendritic structure height is 540 nm, diameter in the base and apex is 100 and 8 nm, respectively, whereas the sizes of „branches“ are from 100 to 10 nm depending on position.

Numerical EF was estimated using the following equation [74]:

$$\mathrm{EF}_{\mathrm{calc}} = \frac{1}{S}\iint\limits_S \frac{|\mathbf{E}|^4}{|\mathbf{E_0}|^4}\,dS, \tag{4}$$

where $\mathbf{E}$ and $\mathbf{E_0}$ are local and incident electric field vectors, respectively; S is the integration surface at 0.1 nm from the air/Ag interface.

Thus, the numerical value of $\mathrm{EF}_{\mathrm{calc}}$ on 633 nm or the model shown in Figure 7, *a* is equal to $5.2 \cdot 10^7$, and for the model consisting of two nanostructures (Figure 7, *b*) $\mathrm{EF}_{\mathrm{calc}}$ was equal to $8 \cdot 10^6$.

Conclusion

SERS substrates, representing dendritic Ag nanostructures, were obtained by chemical reduction of $AgNO_3$ on the c-Si surface with different Ag deposition times.

The limit of detection of brilliant green from the structures studied herein was equal to 10^{-12} M. It was found that the highest intensity of the Raman signal is observed from sample S1 (40 s, 259 nm), then from S2 (60 s, 627 nm), and substrate S3 (90 s, 1084 nm) demonstrates the lowest enhancement, which is probably associated with the

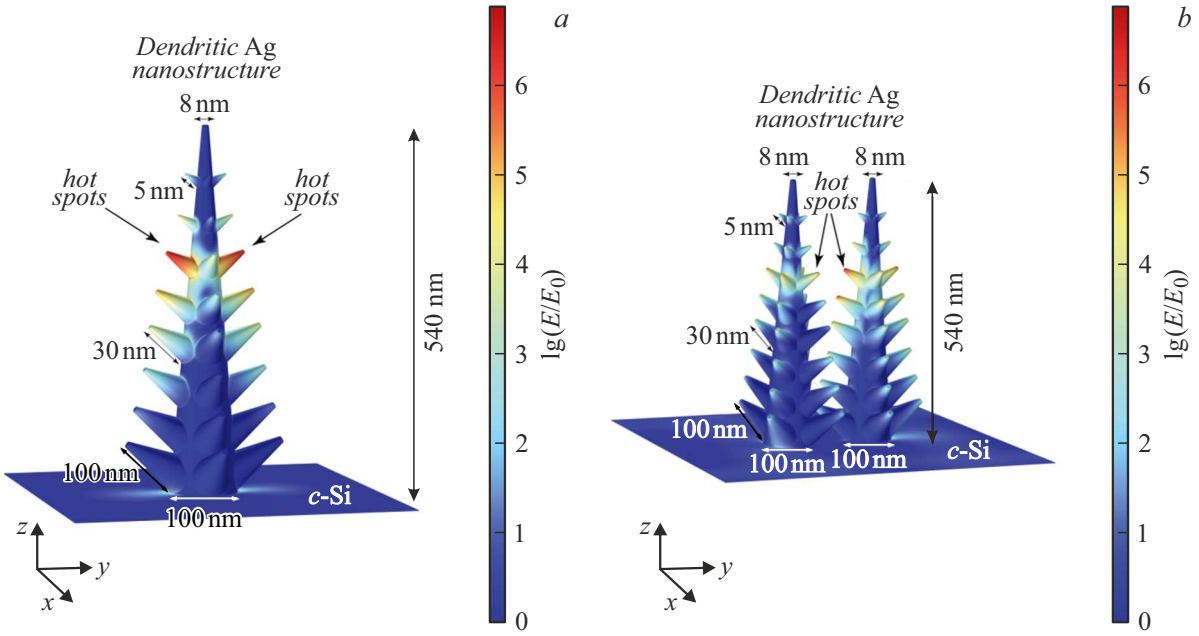

Figure 7. Numerical simulation of electric field strength distribution of the incident plane electromagnetic wave at normal angle to one (*a*) and two (*b*) Ag dendrites on the *c*-Si substrate. Color shows value of $\lg(E/E_0)$, where E is the local electric field and E_0 is the incident electric field, respectively.

structure morphology. Experimental enhancement factors from the structures under study with the applied analyte for sample S1 — $1.14 \cdot 10^8$, for S2 — $7.8 \cdot 10^7$, and for S3 — $1.73 \cdot 10^7$.

COMSOL Multiphysics software suite was used to determine qualitatively the positions of „hot spots“ of the structures and to calculate the enhancement factor on 633 nm that is equal to $5.2 \cdot 10^7$ for the model of one standing Ag nanodendrite, and $8 \cdot 10^6$ for the model of two dendrites.

The SERS studies demonstrate high degree of analyte detection on the fabricated structures. The numerical calculations and experimental data unambiguously show that these structures are very promising as SERS substrates for detection of various triphenylmethane dyes at extremely low concentrations.

Funding

The work was supported by the Russian Science Foundation Grant № 24-22-00334.

Conflict of interest

The authors declare that they have no conflict of interest.

References

[1] R. Kant. Natural Science, **4** (1), 22 (2012). DOI: 10.4236/ns.2012.41004

[2] A. Ajmal, I. Majeed, R.N. Malik, H. Idriss, M.A. Nadeem. RSC Adv., **4** (70), 37003 (2014). DOI: 10.1039/C4RA06658H

[3] K. Hunger. In: *Industrial Dyes: Chemistry, Properties, Applications*, ed. by K. Hunger (Wiley Online Books, 2002), DOI: 10.1002/3527602011.ch1

[4] A.V. Sorokin, A.A. Komarov. Veterinariya, **9**, 1 (55). (in Russian) DOI: 10.30896/0042-4846.2020.23.1.54-60

[5] S.R. Couto. Biotechnol. Adv., **27** (3), 227 (2009). DOI: 10.1016/j.biotechadv.2008.12.001

[6] B.K. Nandi, A. Goswami, M.K. Purkait. J. Hazard. Mater., **161** (1), 387 (2009). DOI: 10.1016/j.jhazmat.2008.03.110

[7] A. Mittal, D. Kaur, J. Mittal. J. Colloid Interface Sci., **326** (1), 8 (2008). DOI: 10.1016/j.jcis.2008.07.005

[8] T. Gessner, U. Mayer. In: *Ullmann's Encyclopedia of Industrial Chemistry*, ed. by Claudia Ley (Wiley-VCH, 2000), DOI: 10.1002/14356007.a27_179

[9] J. Liu, Q. Zhao, W. Cao, H. Zhao, J. Cheng, B. Li, X. Yang. Microchem. J., **158**, 105275 (2020). DOI: 10.1016/j.microc.2020.105275

[10] N. López-Gutiérrez, R. Romero-González, V.J.L. Martínez, A.G. Frenich. Anal. Methods, **5** (14), 3434 (2013). DOI: 10.1039/C3AY40485D

[11] W.C. Andersen, S.B. Turnipseed, C.M. Karbiwnyk, R.H. Lee, S.B. Clark, W.D. Rowe, M.R. Madson, K.E. Miller. Anal. Chim. Acta, **637** (1–2), 279 (2009). DOI: 10.1016/j.aca.2008.09.041

[12] W. Przystaś, E. Zabłocka-Godlewska, E. Grabińska-Sota. Water Air Soil Pollut., **223**, 1581 (2012). DOI: 10.1007/s11270-011-0966-7

[13] W. Przystaś, E. Zabłocka-Godlewska, E. Grabińska-Sota. Water Air Soil Pollut., **224**, 1534 (2013). DOI: 10.1007/s11270-013-1534-0

[14] Y.-Q. Liu, N. Maulidiany, P. Zeng, S. Heo. Chemosphere, **263**, 128312 (2021). DOI: 10.1016/j.chemosphere.2020.128312
[15] X. Lu, C. Qiman, N. Xinkai, Z. Yilin, C. Yu'e, H. Qing, L. Miaoqing, W. Shuang, L. Jihong. Molecules, **28** (14), 5401 (2023). DOI: 10.3390/molecules28145401
[16] H. Yi, W. Qu, W. Huang. Microchim. Acta, **160**, 291 (2008). DOI: 10.1007/s00604-007-0814-z
[17] Y. Zhou, X. Li, Z. Pan, B. Ye, M. Xu. Food Anal. Methods, **12**, 1246 (2019). DOI: 10.1007/s12161-019-01459-x
[18] G. Singh, T. Koerner, J.-M. Gelinas, M. Abbott, B. Brady, A.-C. Huet, C. Charlier, P. Delahaut, S.B. Godefroy. Food Addit. Contam. Part A, **28** (6), 731 (2011). DOI: 10.1080/19440049.2011.567360
[19] K. Mitrowska, A. Posyniak, J. Zmudzki. J. Chromatogr. A, 1089 (1−2), 187 (2005). DOI: 10.1016/j.chroma.2005.07.004
[20] M. Tang, L. Qin, M. Luo, H. Shen, S.-Z. Kang, T. Zhang, X. Li. J. Environ. Chem. Eng., **10** (3), 108040 (2022). DOI: 10.1016/j.jece.2022.108040
[21] A.A. Ermina, N.S. Solodovchenko, V.S. Levitskii, N.A. Belskaya, S.I. Pavlov, V.O. Bolshakov, V.A. Tolmachev, Yu.A. Zharova. Mater. Sci. Semicond. Process., **169**, 107861 (2024). DOI: 10.1016/j.mssp.2023.107861
[22] J. Jiang, Q. Shen, P. Xue, H. Qi, Y. Wu, Y. Teng, Y. Zhang, Y. Liu, X. Zhao, X. Liu. ChemistrySelect, **5** (1), 354 (2020). DOI: 10.1002/slct.201903924
[23] J. Langer, D.J. de Aberasturi, J. Aizpurua, R.A. Alvarez-Puebla, B. Auguié, J.J. Baumberg, G.C. Bazan, S.E.J. Bell, A. Boisen, A.G. Brolo, J. Choo, Dana Cialla-May, V. Deckert, L. Fabris, K. Faulds, F.J. García de Abajo, R. Goodacre, D. Graham, A.J. Haes, Ch.L. Haynes, Ch. Huck, T. Itoh, M. Käll, J. Kneipp, N.A. Kotov, H. Kuang, E.C. Le Ru, H.K. Lee, J.-F. Li, X. Yi Ling, S.A. Maier, Th. Mayerhöfer, M. Moskovits, K. Murakoshi, J.-M. Nam, Sh. Nie, Y. Ozaki, I. Pastoriza-Santos, J. Perez-Juste, J. Popp, A. Pucci, S. Reich, B. Ren, G.C. Schatz, T. Shegai, S. Schlücker, L.-L. Tay, K.G. Thomas, Zh.-Q. Tian, R.P. Van Duyne, T. Vo-Dinh, Y. Wang, K.A. Willets, Ch. Xu, H. Xu, Y. Xu, Y.S. Yamamoto, B. Zhao, L.M. Liz-Marzán. ACS Nano, **14** (1), 28 (2020). DOI: 10.1021/acsnano.9b04224
[24] X. Zheng, Z. Ye, Z. Akmal, C. He, J. Zhang, L. Wang. Chem. Soc. Rev., **53** (2), 656 (2024). DOI: 10.1039/D3CS00462G
[25] R. Peng, T. Zhang, S. Yan, Y. Song, X. Liu, J. Wang. Nanomaterials, **13** (22), 2968 (2023). DOI: 10.3390/nano13222968
[26] W. Li, X. Zhao, Z. Yi, A.M. Glushenkov, L. Kong. Anal. Chim. Acta, **984**, 19 (2017). DOI: 10.1016/j.aca.2017.06.002
[27] K. Kneipp, Y. Wang, H. Kneipp, L.T. Perelman, I. Itzkan, R.R. Dasari, M.S. Feld. Phys. Rev. Lett., **78** (9), 1667 (1997). DOI: 10.1103/PhysRevLett.78.1667
[28] L. Long, W. Ju, H.-Y. Yang, Z. Li. ACS Mater. Au, **2** (5), 552 (2022). DOI: 10.1021/acsmaterialsau.2c00005
[29] M.S. Goh, Y.H. Lee, S. Pedireddy, I.Y. Phang, W.W. Tjiu, J.M.R. Tan, X.Y. Ling. Langmuir, **28** (40), 14441 (2012). DOI: 10.1021/la302795
[30] Z. Zhang, J. Wang, K.B. Shanmugasundaram, B. Yeo, A. Möller, A. Wuethrich, L.L. Lin, M. Trau. Small, **16** (13), 1905614 (2020). DOI: 10.1002/smll.201905614
[31] K. Prigoda, A. Ermina, V. Bolshakov, A. Tabarov, V. Levitskii, O. Andreeva, A. Gazizulin, S. Pavlov, D. Danilenko, V. Vitkin, Yu. Zharova. Opt. Mater., **149**, 114977 (2024). DOI: 10.1016/j.optmat.2024.114977
[32] A. Tabarov, V. Vitkin, O. Andreeva, A. Shemanaeva, E. Popov, A. Dobroslavin, V. Kurikova, O. Kuznetsova, K. Grigorenko, I. Tzibizov, A. Kovalev, V. Savchenko, A. Zheltuhina, A. Gorshkov, D. Danilenko. Biosensors, **12** (12), 1065 (2022). DOI: 10.3390/bios12121065
[33] S. Aitekenov, A. Sultangaziyev, A. Boranova, A. Dyussupova, A. Ilyas, A. Gaipov, R. Bukasov. Sensors, **23** (3), 1605 (2023). DOI: 10.3390/s23031605
[34] T. Liyanage, A. Rael, S. Shaffer, S. Zaidi, J.V. Goodpaster, R. Sardar. Analyst, **143** (9), 2012 (2018). DOI: 10.1039/C8AN00008E
[35] J.B.M. Parambath, G. Kim, C. Han A.A. Mohamed. Res. Chem. Intermed., **49**, 1259 (2023). DOI: 10.1007/s11164-022-04913-4
[36] H. Sun, X. Li, Z. Hu, C. Gu, D. Chen, J. Wang, B. Li, T. Jiang, X. Zhou. Appl. Surf. Sci., **556**, 149748 (2021). DOI: 10.1016/j.apsusc.2021.149748
[37] X. He, X. Zhou, Y. Liu, X. Wang. Sens. Actuators B Chem., **311**, 127676 (2020). DOI: 10.1016/j.snb.2020.127676
[38] I.B. Ansah, S.H. Lee, C. Mun, J.-Y. Yang, J. Park, S.-Y. Nam, S. Lee, D.-H. Kim, S.-G. Park. Sens. Actuators B Chem., **379**, 133172 (2023). DOI: 10.1016/j.snb.2022.133172
[39] M.K. Pham, D.T.N. Nga, Q.D. Mai, V.M. Tien, N.Q. Hoa, V.D. Lam, H.A. Nguyen, A.-T. Le. Anal. Methods, **15** (39), 5239 (2023). DOI: 10.1039/D3AY01374J
[40] A.A. Ermina, N.S. Solodovchenko, K.V. Prigoda, V.S. Levitskii, V.O. Bolshakov, M.Yu. Maximov, Yu.M. Koshtyal, S.I. Pavlov, V.A. Tolmachev, Yu.A. Zharova. Appl. Surf. Sci., **608**, 155146 (2023). DOI: 10.1016/j.apsusc.2022.155146
[41] X. Wang, X. Zhu, Y. Chen, M. Zheng, Q. Xiang, Z. Tang, G. Zhang, H. Duan. ACS Appl. Mater. Interfaces, **9** (36), 31102 (2017). DOI: 10.1021/acsami.7b08818
[42] J. Chen, Y. Huang, P. Kannan, L. Zhang, Z. Lin, J. Zhang, T. Chen, L. Guo. Anal. Chem., **88** (4), 2149 (2016). DOI: 10.1021/acs.analchem.5b03735
[43] Z. Deng, X. Chen, Y. Wang, E. Fang, Z. Zhang, X. Chen. Anal. Chem., **87** (1), 633 (2015). DOI: 10.1021/ac503341g
[44] A. Milewska, V. Zivanovic, V. Merk, U.B. Arnalds, Ó.E. Sigurjónsson, J. Kneipp, K. Leosson. Biomed. Opt. Express, **10**, 6172 (2019). DOI: 10.1364/BOE.10.006172
[45] K. Prigoda, A. Ermina, V. Bolshakov, D. Nazarov, I. Ezhov, O. Lutakov, M. Maximov, V. Tolmachev, Y. Zharova. Coatings, **12** (11), 1748 (2022). DOI: 10.3390/coatings12111748
[46] D.A. Nazarovskaia, P.A. Domnin, O.D. Gyuppenen, I.I. Tsiniaikin, S.A. Ermolaeva, K.A. Gonchar, L.A. Osminkina. Bull. Russ. Acad. Sci. Phys., **87** (1), 41 (2023). DOI: 10.1134/S1062873823704385
[47] A.A. Ermina, N.S. Solodovchenko, K.V. Prigoda, V.S. Levitskii, S.I. Pavlov, Yu.A. Zharova. Semicond, **57** (4), 241 (2023). DOI: 10.61011/SC.2023.04.56420.07k
[48] Y. Lu, C.-Y. Zhang, D.-J. Zhang, R. Hao, Y.-W. Hao, Y.-Q. Liu. Chin. Chem. Lett., **27** (5), 689 (2016). DOI: 10.1016/j.cclet.2016.01.032
[40] A. Khorshidi, N. Mardazad. Res. Chem. Intermed., **42**, 7551 (2016). DOI: 10.1007/s11164-016-2552-5
[50] L.A. Osminkina, O. Žukovskaja, S.N. Agafilushkina, E. Kaniukov, O. Stranik, K.A. Gonchar, D. Yakimchuk, V. Bundyukova, D.A. Chermoshentsev, S.A. Dyakov, N.A. Gippius, K. Weber, J. Popp, D. Cialla-May, V. Sivakov. Appl. Surf. Sci., **507**, 144989 (2020). DOI: 10.1016/j.apsusc.2019.144989

[51] D. Ge, J. Wei, J. Ding, J. Zhang, C. Ma, M. Wang, L. Zhang, S. Zhu. ACS Appl. Nano Mater., **3** (3), 3011 (2020). DOI: 10.1021/acsanm.0c00296
[52] S.A. Razek, A.B. Ayoub, M.A. Swillam. Sci. Rep., **9**, 13588 (2019). DOI: 10.1038/s41598-019-49896-2
[53] Z.-Y. Li. Adv. Opt. Mater., **6** (16), 1701097 (2018). DOI: 10.1002/adom.201701097
[54] T.C. Dao, T.Q.N. Luong, T.A. Cao, M.K. Ngoc. Comm. Phys., **32** (2), 201 (2022). DOI: 10.15625/0868-3166/16113
[55] C. Bi, Y. Song, H. Zhao, G. Liu. RSC Adv., **12** (30), 19571 (2022). DOI: 10.1039/D2RA02651A
[56] A.M. Schwartzberg, C.D. Grant, A. Wolcott, C.E. Talley, T.R. Huser, R. Bogomolni, J.Z. Zhang. J. Phys. Chem. B, **108** (50), 19191 (2004). DOI: 10.1021/jp048430p
[57] Y. Zharova, A. Ermina, S. Pavlov, Y. Koshtyal, V. Tolmachev. Phys. Status Solidi A, **216** (17), 1900318 (2019). DOI: 10.1002/pssa.201900318
[58] V.A. Tolmachev, E.V. Gushchina, I.A. Nyapshaev, Yu.A. Zharova. Thin Solid Films, **756**, 139352 (2022). DOI: 10.1016/j.tsf.2022.139352
[59] V.A. Tolmachev, Yu.A. Zharova, A.A. Ermina, V.O. Bolshakov. Opt. Spectr., **130** (2), 238 (2022). DOI: 10.21883/EOS.2022.02.53215.2668-21
[60] T.C. Dao, T.Q.N. Luong, T.A. Cao, M.K. Ngoc., V.L. Van. Adv. Nat. Sci: Nanosci. Nanotechnol., **7** (1), 015007 (2016). DOI: 10.1088/2043-6262/7/1/015007
[61] V.S. Vendamani, S.V.S. Nageswara Rao, A.P. Pathak, V.R. Soma. RSC Adv., **10** (73), 44747 (2020). DOI: 10.1039/D0RA08834J
[62] M.V. Mandke, S.-H. Han, H.M. Pathan. Cryst. Eng. Comm., **14** (1), 86 (2012). DOI: 10.1039/c1ce05791j
[63] W. Ye, C. Shen, J. Tian, C. Wang, C. Hui, H. Gao. Solid State Sci., **11** (6), 1088 (2009). DOI: 10.1016/j.solidstatesciences.2009.03.001
[64] T.C. Dao, T.Q.N. Luong, Q.N. Truc. RSC Adv., **10** (67), 40940 (2020). DOI: 10.1039/d0ra08060h
[65] T.A. Witten, L.M. Sander. Phys. Rev. Lett., **47** (19), 1400 (1981). DOI: 10.1103/PhysRevLett.47.1400
[66] Z. Yang, W.W. Tjiu, W. Fan, T. Liu. Electrochim. Acta, **90**, 400 (2013). DOI: 10.1016/j.electacta.2012.12.038
[67] X. Qin, H. Wang, X. Wang, Z. Miao, Y. Fang, Q. Chen, X. Shao. Electrochim. Acta, **56** (9), 3170 (2011). DOI: 10.1016/j.electacta.2011.01.058
[68] R.W.G. Wyckoff. *Crystal Structures* (Interscience publishers, NY., 1963)
[69] K. Uchinokura, T. Sekine, E. Matsuura. Solid State Commun., **11** (1), 47 (1972). DOI: 10.1016/0038-1098(72)91127-1
[70] J. Chowdhury, M. Ghosh. J. Colloid Interface Sci., **277** (1), 121 (2004). DOI: 10.1016/j.jcis.2004.04.030
[71] Y. Wang, D. Li, P. Li, W. Wang, W. Ren, S. Dong, E. Wang. J. Phys. Chem. C, **111** (45), 16833 (2007). DOI: 10.1021/jp074519u
[72] P. Simakova, E. Kocivsova, M. Prochazka. J. Nanomater., **2021**, 4009352 (2021). DOI: 10.1155/2021/4009352
[73] E.C. Le Ru, E.J. Blackie, M. Meyer, P.G. Etchegoin. J. Phys. Chem. C, **111** (37), 13794 (2007). DOI: 10.1021/jp0687908
[74] P. Hildebrandt, M. Stockburger. J. Phys. Chem., **88** (24), 5935 (1984). DOI: 10.1021/j150668a038

Translated by E.Ilinskaya